TITLE PAGE

Citation Format:

Maffeis G, Witteveen M, Jong LS, Damagatla V, Sterenborg HJCM, Post AL, Dalla Mora A, Ruers TJM, Taroni P. Optical Characterization of Coconut Oil from 600 nm to 1600 nm for Use as a Tissue Phantom. Appl Spectrosc. 2026 Apr;80(4):327-337. doi: 10.1177/00037028261419837. Epub 2026 Jan 20. PMID: 41556426.

Abstract link:

https://journals.sagepub.com/doi/10.1177/00037028261419837

Optical characterization of coconut oil from 600 nm to 1600 nm for use as a tissue phantom

Giulia Maffeis[1], Mark Witteveen[2], Lynn-Jade S. Jong[2], Vamshi Damagatla[1], Henricus J. C. M. Sterenborg[2], Anouk Laetitia Post[2], Alberto Dalla Mora[1], Theo J.M. Ruers[2], Paola Taroni[1]

[1]Department of Physics, Politecnico di Milano, Milan, Italy
[2]Department of Surgery, The Netherlands Cancer Institute, Amsterdam, the Netherlands

ABSTRACT

Optical phantoms are widely used to characterize diffuse optical setups and data analysis methods for in vivo/ex vivo measurements. Coconut oil is an interesting compound to use in phantoms, because it could be used to model lipidic tissues, such as the one in breast tissue. In this paper, we measure the absorption and scattering spectra of coconut oil from 600 to 1600 nm, encompassing the so-called "therapeutic window". To cover the entire range, we exploit a supercontinuum pulsed laser and a superconducting nanowire single photon detector operating in the time domain. Finally, we demonstrate the use of a homogeneous coconut oil phantom to characterize a hyperspectral continuous-wave setup.

KEYWORDS

Diffuse optics, coconut oil, biological tissues, tissue phantom.

1 INTRODUCTION

One of the goals of diffuse optical measurements is the estimation of the absorption ($\mu_a(\lambda)$) and reduced scattering ($\mu_s'(\lambda)$), from now on referred to as scattering) properties of turbid media based on their response to red and near-infrared light, with wavelength (λ) ranging from 600 nm to 1600 nm.[1–3] In that spectral range, biological tissues typically exhibit properties of a turbid medium, thereby providing a compelling avenue for exploration within the field of biomedical applications. In this case, the conversion of the optical properties into composition (*i.e.*, constituent concentrations, related to absorption) and microstructure (*i.e.*, micro-organelles density and size, related to scattering) parameters through the Lambert-Beer law and the Mie empirical model,[4] respectively, gives the opportunity to assess the health status of a tissue or its functional reaction to an external stimulus. Indeed, diffuse optics already proved promising for example for breast cancer diagnosis and therapy monitoring,[5,6] surgical margin assessment for lungs,[7,8] rectum[9] and oral cavity,[10,11] brain activity detection,[12–14] assessment of muscle function and composition.[15,16]

However, an efficient measurement and interpretation of *in vivo* results is not straightforward, primarily due to the strong intra- and inter-subject variability. Therefore, a thorough and rigorous laboratory characterization of the system (in this work meant as the ensemble of setup, measurement conditions and data analysis methods) is required before *in vivo* or even *ex vivo* measurements.

An efficient methodological approach should envision a sequence of tests, going from the simplest to the most articulated one, in preparation for a clinical study, whenever feasible. A possible operating pipeline could be:

- Simulations

- Phantoms aimed at mimicking absorption and scattering properties (*e.g.*, resin,[17,18] silicone,[17,19,20] intralipid,[21–24] 3D filament[25–27])
- Phantoms aimed at mimicking constituent concentrations, reproducing as fairly as possible the composition and structure of the final *in vivo* setting (*e.g.*, red meat, lard, tendon[28,29])
- *Ex vivo* surgical specimens
- Initial *in vivo* tests on healthy volunteers
- *In vivo* measurements on patients.

Tests on phantoms therefore represent an essential part of the validation procedure of a diffuse optical system,[30,31] underlying the importance of the availability of a large variety of technologies to fabricate them.

In this regard, in this paper we propose coconut oil as material to fabricate phantoms, playing the role of fat tissue. Coconut oil has the advantage that it is a solid, is characterized by both scattering and absorption, and can be easily moulded into various shapes. It has already been employed, even if on limited occasions, in phantom tests with diffuse optical instrumentations.[32,33] For instance, it was used in studies on liver steatosis,[34] for tumour detection[35] and to replace Intralipid.[36] However, a full characterization of the absorption and scattering coefficients from 600 nm to 1600 nm is still missing.[31,32.] In this paper, we provide the absorption and scattering spectra of coconut oil, which will enable its use as a standard for phantoms.

Coconut oil is cheap, easy to find even at the supermarket, homogeneous, and it enables the fabrication of complex structures in terms of shape and assembly (*e.g.*, inclusion in a homogeneous background, multilayer).

There are different possible approaches to diffuse optics to estimate the optical properties of coconut oil. We will investigate the time and Continuous Wave (CW) domains. The former allows one to disentangle absorption and scattering with a single measurement, at the expenses of a high-cost and articulated setup. The latter can utilize simpler hardware, but demands special attention during fitting to decouple the two contributions.

For these reasons, to harness the strengths of each approach fully, the work is divided into two parts.

The first part thoroughly investigates the primary goal of this paper: to assess $\mu_a(\lambda)$, and $\mu_s'(\lambda)$ of solid-state coconut oil (temperature lower than 25°C) at optimized measurement conditions and define a reference for the extinction coefficients in the Lambert-Beer equation. These values could then be used by anyone interested in the coconut absorption spectrum from 600 to 1600 nm. This part involves the use of a time-resolved system, which is a well-established option to estimate the absolute values of the optical coefficients.

In the second part, we check the quality of the retrieved $\mu_a(\lambda)$ measuring a homogeneous coconut phantom with a hyperspectral CW system. Here, the goal is to test whether the fitting procedure, based on the use of the measured absorption spectrum as extinction coefficient, correctly recognizes the phantom composition.

2 MATERIALS AND METHODS

2.1 Assessment of the optical properties of coconut oil

The goal of the following diffuse optical measurements is to characterize the absorption and scattering coefficients of coconut oil from 600 to 1600 nm as accurately as possible. Absorption is related to the chemical composition of the medium and can be quantified through the concentrations of its constituents. In the case of pure coconut oil, we expect it to consist entirely of lipids.

The scattering spectrum, on the other hand, provides insights into the microstructure of the medium. In biological tissues, 'microstructure' refers to the organization of microscopic scatterers—such as particles, organelles, cell membranes, mitochondria, and collagen fibers—which influence how light travels through the material. For coconut oil, microstructure may involve the distribution of fat particles, the presence of air bubbles, and the degree of crystallinity. Notably, as temperature increases (and crystallinity decreases), scattering tends to diminish.[37,38]

As mentioned above, an efficient approach to assess the two optical properties simultaneously, minimizing their potential coupling, is to use a time-resolved diffuse optics setup.[39]

The setup and data analysis methods for measurements in the time domain employed to estimate the absorption and scattering spectra of coconut oil are described in the following sections.

2.1.1 Broadband time-resolved setup

The main constraint for the design of the time-resolved setup for this application is the extensive spectral range (600–1600 nm). To cover it, a pulsed supercontinuum laser operating at 80 MHz (FIU-15, NKT Photonics, Denmark) and a superconducting nanowire single photon detector (SNSPD - Eos, Single Quantum, Netherlands) have been employed (Figure 1).

Other than the source and the detector, the components of the device are a rotating Pellin-Broca prism to select single λs, a variable Neutral Density filter (ND) to modulate light intensity, and a board for Time-Correlated Single-Photon Counting (TCSPC - SPC-130, Becker and Hickl, Germany) to reconstruct the Distribution of photon Times Of Flight (DTOF). Light is delivered to the sample through a 200-µm core step index fiber and collected from the sample through a 1-mm core step index fiber.

The choice of the fiber core diameter, especially on the collection side, introduces a trade-off between signal level and temporal resolution: the smaller it is the better the temporal resolution, but the lower the signal. Also, in time domain, absorption mainly affects the DTOF shape: a higher absorption produces a faster decay of the tail in the DTOF, thus narrowing its shape. Therefore, when absorption is high, the DTOF might be similar to the Instrument Response Function (IRF) and it is important to have an adequate temporal resolution to avoid this risk. Considering our case, the absorption coefficients could exceed 1 cm^{-1} in the 600-1600 nm range, which explains the different fiber core diameter: small on the source side for higher temporal resolution and bigger on the detection side for better signal collection.

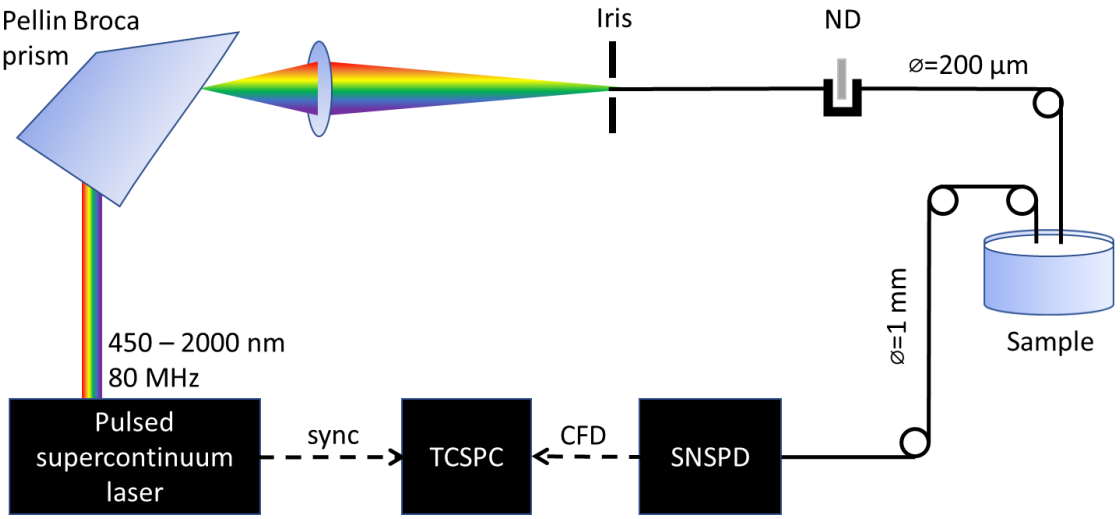

Figure 1: Broadband time-resolved experimental setup. Picosecond laser pulses are sent to the sample, after λ selection through a rotating Pellin-Broca prism and intensity tuning through a variable neutral density filter (ND). The signal is collected by a detector (SNSPD) and its output is delivered to a TCSPC board through a Constant Fraction Discriminator (CFD).

2.1.2 Coconut oil phantoms for absorption assessment

For reproducibility purposes, 15 phantoms were fabricated, consisting of 3 brands and 5 samples for each brand. Table 1 reports the composition data and the melting temperature for each brand. Coconut oil was melted at 60°C and poured in cylindrical polypropylene jars (melting temperature between 130 and 171°C)[40], so that each phantom had a diameter of 11 cm and a height of about 3 cm. After cooling to room temperature, the coconut oil was stored in the refrigerator at about 8°C. Figure 2 depicts the phantoms while coconut oil is still melted, highlighting the different colours of the different brands. Such difference in colour is not evident at solid state.

For the sake of completeness, we include in Table 1 also the information of the fourth brand of coconut oil, used to validate the absorption spectrum retrieved from the other 3 brands. All coconut oil brands were purchased from a grocery shelf, one of our goals being the use of easily accessible materials.

Table 1: Data about phantom composition and features.

	Brand 1	**Brand 2**	**Brand 3**	**Brand 4**
Name	Planète au naturel	Cibo crudo	Naturale bio	Kruidvat
Origin	Vietnam	Philippines	Sri Lanka	Non EU agriculture
Features	100% virgin, pure and biologic; cold-pressed	100% virgin, pure and biologic; cold-pressed	100% virgin, pure and biologic; cold-pressed	100% pure, organic, de-odorised
Melting temperature	25°C	25°C	23°C	25°C
Composition for 100 g				

- **Fat (of which saturated fatty acids)**	100 g (86.5 g)	100 g (91 g)	100 g (92 g)	100 g (91 g)
- **Carbohydrates (of which sugar)**	0 g (0 g)	0 g (0 g)	0 g (0 g)	0 g (0 g)
- **Proteins**	0 g	0 g	0 g	0 g
- **Salt**	0 g	0 g	0 g	0 g

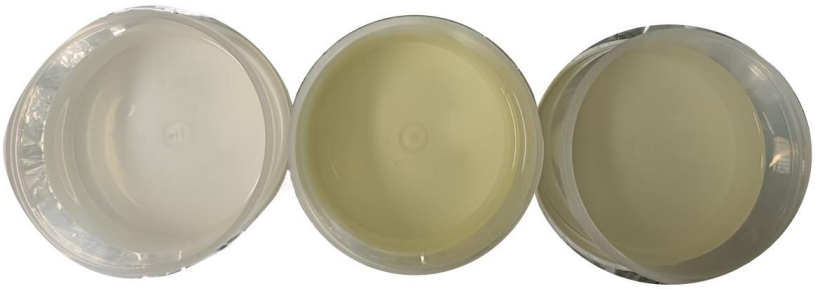

Figure 2: Photograph of phantoms of the 3 different brands (brand 1 on the left, brand 2 in the center, brand 3 on the right), while coconut oil is melted.

2.1.3 Measurements protocol

The complete set of 15 phantoms was measured four times over a period of eight days (on days 1, 4, 6, and 8) to assess the measurement reproducibility. Each coconut oil phantom was removed from the refrigerator only for the duration of the acquisition and placed in a water and ice bath to keep it at about 16°C during the acquisitions. The laser intensity was modulated with the ND filter to achieve a count-rate of about 100 kcps in order to operate in single photon regime. All measurements were performed at 1 cm inter-fiber distance, limited by the low signal-to-noise ratio at the highest absorption peaks. Acquisitions were carried out with an integration time of 1 s at a step of 5 nm, taking about 5 minutes. It is important to consider that the spectral resolution of the setup ranges from 2 nm in the visible range to about 10 nm in the infrared one.

2.1.4 Spectra data analysis

Data were processed with two different methods.

The first method ("method 1") is fully based on experimental data and consists in retrieving the absorption and reduced scattering coefficients of coconut oil as a function of λ by applying the solution to the diffusion equation for a homogeneous semi-infinite medium in reflectance geometry in time domain.[41] The theoretical DTOF is convolved with the IRF to account for system effects.

The refractive index is one of the parameters required by the fitting procedure. For coconut oil, we used the relation proposed in Ref. [42], where n = 1.44 at 600-1600 nm. The portion of each output pulse considered for the fit was from 50% in amplitude with respect to the peak on the rising edge, to 1% on the tail.

The second method ("method 2") is hybrid and based on a four-stage procedure. The first stage coincides with "method 1". However, here $\mu_s'(\lambda)$ is later fitted using an approximation to Mie theory (stage 2), in order to obtain the scattering amplitude (a, related to the scatterers density) and slope (b, related to the scatterers size), with $\lambda_0 = 600$ nm as reference λ:

$$\mu_s'(\lambda) = a\left(\frac{\lambda}{\lambda_0}\right)^{-b}. \qquad (1)$$

The two parameters are then replaced in Eq. (1) to compute $\mu_{s,fit}'(\lambda)$ (stage 3). Therefore, Eq. (1) is used with an inverse approach in stage 2 and a forward approach in stage 3. Finally, $\mu_{s,fit}'(\lambda)$ is involved as a fixed parameter in a fitting procedure similar to "method 1", while $\mu_a(\lambda)$ is the only free parameter (stage 4).

The advantage of method 2 with respect to the fully-experimental method 1 is the smoothing effect on the decreasing exponential behaviour of scattering, with a consequent improvement in absorption estimate.

2.2 Validation of the optical properties of coconut oil

After assessing the absorption spectrum, its quality is tested in a fitting procedure aimed at retrieving the composition of a homogeneous coconut phantom. For this purpose, a CW imaging setup and proper analytical models are used, as described below.

2.2.1 Coconut oil phantom for validation

Figure 3 depicts an example of a solid phantom fabricated with "brand 4" coconut oil (Table 1).
The phantom was produced by melting coconut oil on a hot plate at 60°C, pouring it in a mould and letting it solidify in a refrigerator (8°C) over night. It has a truncated cone shape, with a height of 3 cm and a diameter of 6.5 cm at the top surface. The phantom was measured on 3 different days over a month (Day 1, Day 18, Day 28).

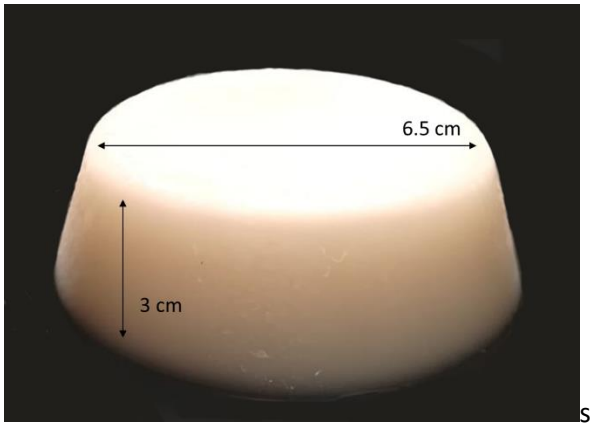

Figure 3: Example of homogeneous coconut phantom used for validation.

2.2.2 CW experimental setup

Diffuse reflection spectra of the phantom were measured with the CW hyperspectral imaging instrumentation described in Ref.[43–46]. The phantom was illuminated by three halogen light sources (2900 K), under an angle of 35°. Then, data were acquired with a push-broom camera, sensitive in the infrared range (Specim VLNIR CL-350-N17E, InGaAs sensor 320 × 256 pixels, 0.5 mm/pixel, ~900-1700 nm, 256 λ, 5 nm step), while the sample was automatically moved by a translational stage.

2.2.3 Phantom data analysis

The output spectra were analysed with the model proposed by Flock et al., suitable for broadband CW measurements in reflectance geometry.[24,47] In particular, the Mie theory (Eq. (1)) and the Lambert-Beer law were replaced in the model to explicit $\mu_a(\lambda)$ and $\mu_s'(\lambda)$. The Lambert-Beer law is expressed by:

$$\mu_a(\lambda) = \sum_i^N \epsilon_i C_i \qquad (2)$$

where ϵ_i is the extinction coefficient of the i^{th} constituent, C_i is its concentration, N is the number of constituents. The fit was performed looking for the concentrations of coconut oil and water, that, being coconut oil a lipidic substance, are characterized by significantly different spectra, with major

absorption peaks in the infrared region. We do not expect to detect any water content. If present, the only contribution could be due to a very superficial layer due to condensation.

The key point of the CW measurements is the use the absorption spectrum previously derived as extinction coefficient $\varepsilon_{coconut}$ for coconut in Eq. (2) and the test of its effectiveness.

Such procedure was applied to 289 pixels composing the hyperspectral image of the coconut phantom, in order to assess reproducibility and robustness.

3 RESULTS AND DISCUSSION

3.1 Determination of the optical properties of coconut oil

Figure 1 and Figure 5 represent the raw (method 1, solid curves) and fitted (method 2, dotted curves) scattering and absorption spectra, respectively, over brands (columns) and days (rows). Each panel depicts the results obtained for the 5 repetitions.

In Figure 4, the two methods return quite consistent results everywhere, except for the 1200 and the 1400 nm peaks. It could be attributed to a coupling between $\mu_a(\lambda)$ and $\mu_s'(\lambda)$ due to the high value of $\mu_a(\lambda)$ in this region, which manifests via noise in scattering. This coupling has already been investigated by Faber et al. in Ref.[48] for haemoglobin. Even a different fitting range of the curve could not fix such distortion. However, the smoother $\mu_{s,fit}'(\lambda)$ used in method 2 compensates for this artefact. This is the reason why Mie theory was applied limited to the 600-950 nm range to retrieve the amplitude and slope parameters.

Figure 5 reflects the fluctuations of Figure 4 around 1200 and 1400 nm. Also, there is a mismatch where $\mu_a < 0.02$ cm^{-1}.

Figure 6 and Figure 7 represent the fitted scattering and absorption spectra of coconut oil obtained through time-resolved diffuse optical measurements, after applying “method 2”. The two figures share the same structure. In the first row, each panel displays three spectra (averaged over the five repetitions) corresponding to the three brands, while the sequence of panels represents the assessment across days. In the second row, each panel shows four spectra (averaged over the five repetitions) corresponding to the four days, and the sequence of panels represents the assessment across brands. In other words, the first and second rows depict the same data, but from complementary perspectives, to emphasize different types of comparison.

Ideally, spectra acquired on different days should overlap, whereas spectra from different brands may exhibit variations due to slight differences in composition. In the figures, however, variations are visible from both perspectives.

Scattering is significantly sensitive to temperature and to the presence of possible inhomogeneities within the sample. In this context, the position of the probe relative to the sample could play a significant role. These factors might explain the observed spread in the spectra, quantified by the amplitude and slope parameters computed using Method 2 and averaged over the spectra shown in each corresponding panel. The average amplitude a is equal to 16.67±3.58 cm^{-1}, with 95% confidence interval for normal distribution [15.76, 17.57] cm^{-1} over 4 days, 3 brands and 5 repetitions. The average slope b is equal to 0.39±0.25, with 95% confidence interval for normal distribution [0.32, 0.45] over 4 days, 3 brands and 5 repetitions.

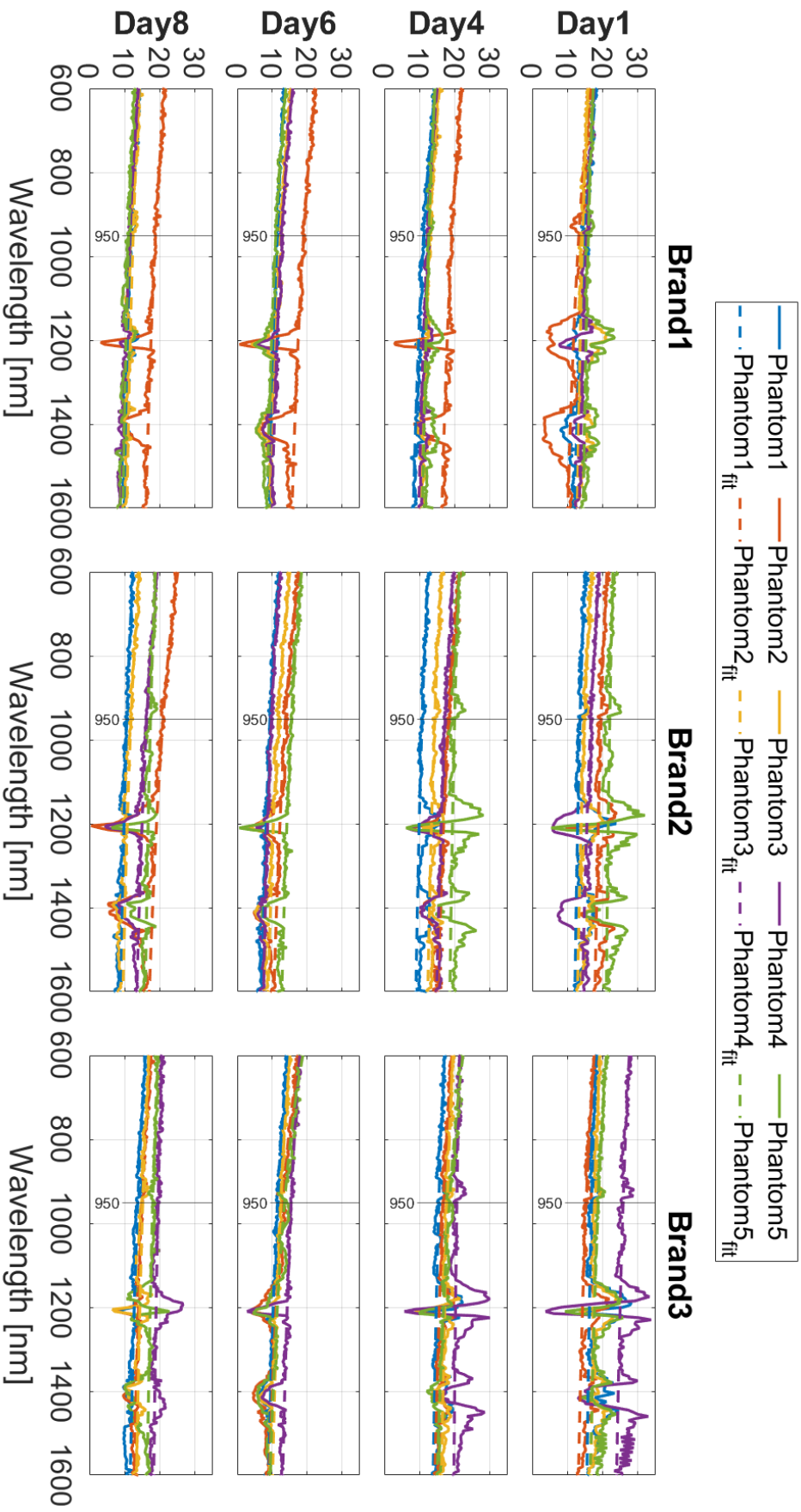

Figure 4: Raw (solid line) and fitted (dotted line) scattering spectra in cm^{-1} over brands (columns) and days (rows). Each panel depicts the results obtained for the 5 repetitions.

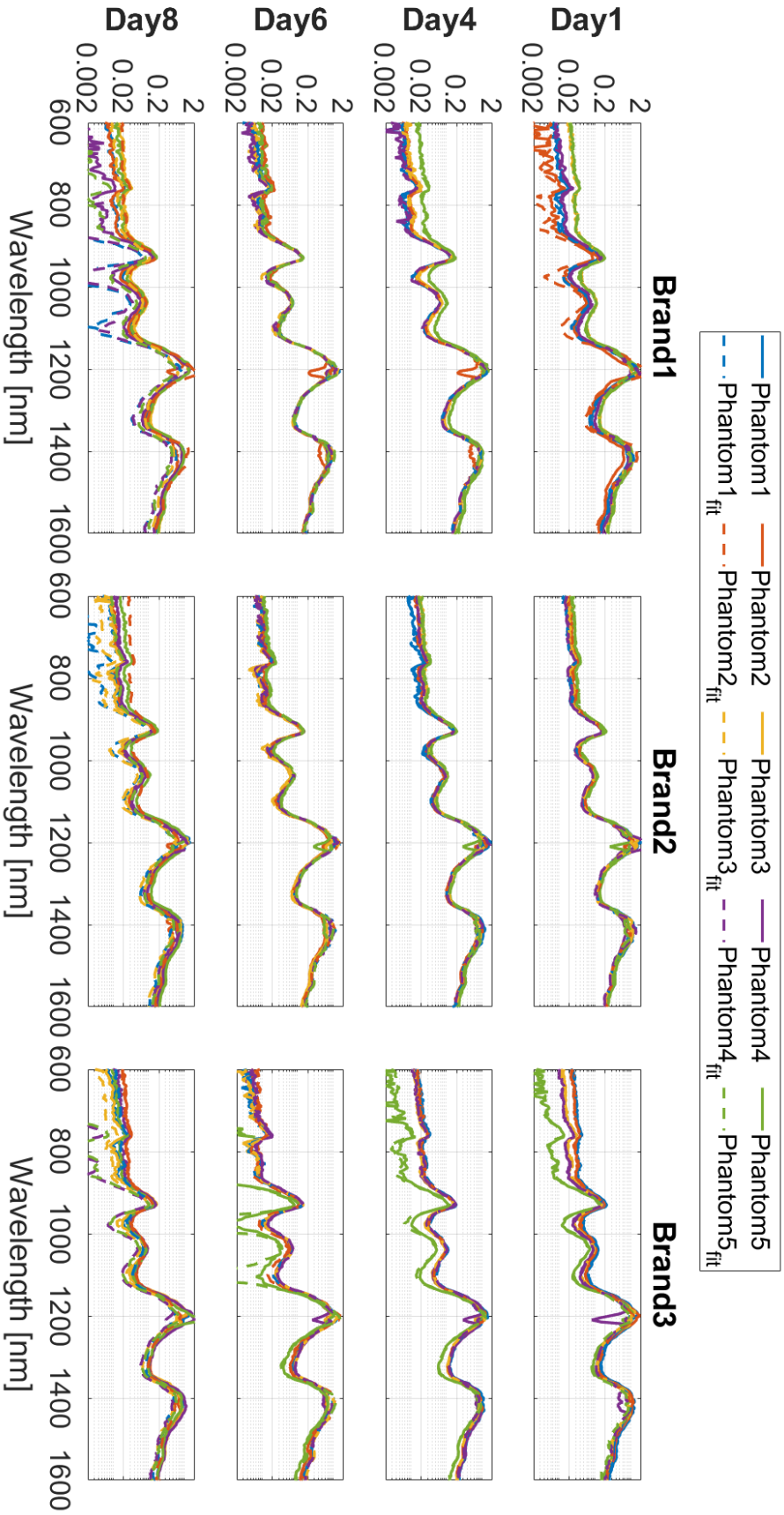

Figure 5: Raw (solid line) and fitted (dotted line) absorption spectra in cm^{-1} over brands (columns) and days (rows). Each panel depicts the results obtained for the 5 repetitions. A logarithmic vertical scale is used.

The variability in absorption across days may again be attributed to some sample inhomogeneity combined with slight changes in the relative positioning of the probe with respect to the sample. Conversely, the different yellowish shades of the various brands (Figure 2) already suggested a degree of variation in absorption, particularly in the initial part of the spectrum. This trend is even more evident in Figure 8, which represent spectra averaged over repetitions and days. Here, "brand 1" (the clearest in Figure 2) at short λ shows consistently lower absorption than "brand 3" (the moderately yellowish one), that in turn shows consistently lower absorption than "brand 2" (the most yellowish). Such difference might be due to subtle, but measurable differences in composition and processing. Another possible explanation is that the sample is not rigorously semi-infinite, as assumed in the analysis. The average spectrum is closer to the one of "brand 3". Brand 1 oscillates between 0.73 cm^{-1} (665 nm) and 1.13 cm^{-1} (1210 nm). Brand 2 oscillated between 0.99 cm^{-1} (1455 nm) and 1.35 cm^{-1} (600 nm). Brand 3 oscillates between 0.85 cm^{-1} (1210 nm) and 1.03 cm^{-1} (1315 nm).

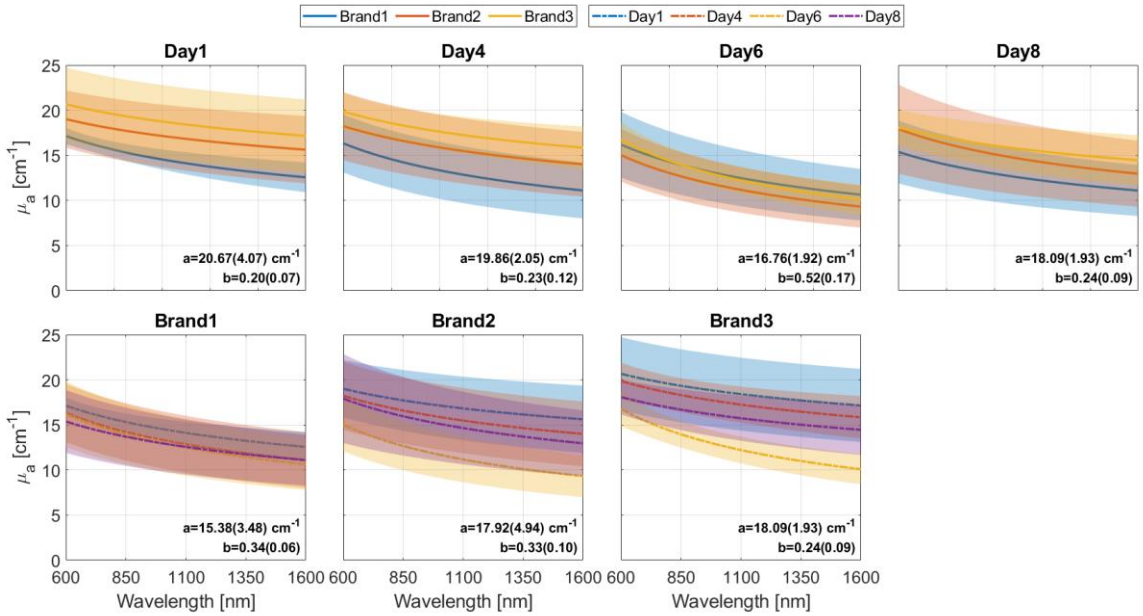

Figure 6: First row: fitted scattering spectra averaged over 5 repetitions, obtained on different days. Second row: fitted scattering spectra averaged over 5 repetitions, obtained for different brands.

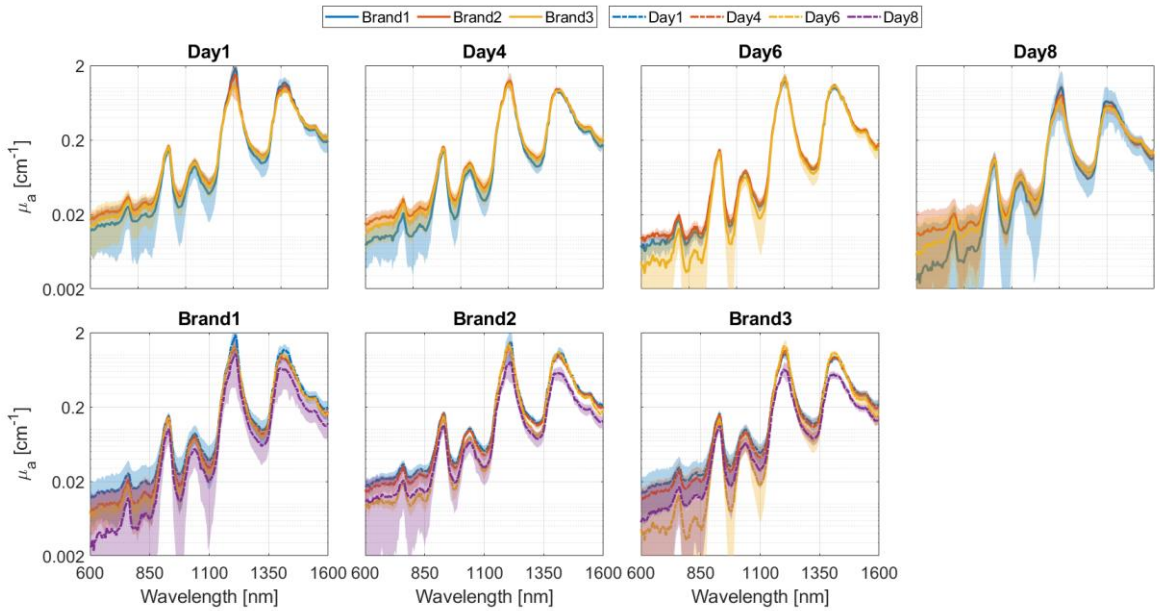

Figure 7: First row: fitted absorption spectra averaged over 5 repetitions, obtained on different days. Second row: fitted absorption spectra averaged over 5 repetitions, obtained for different brands.

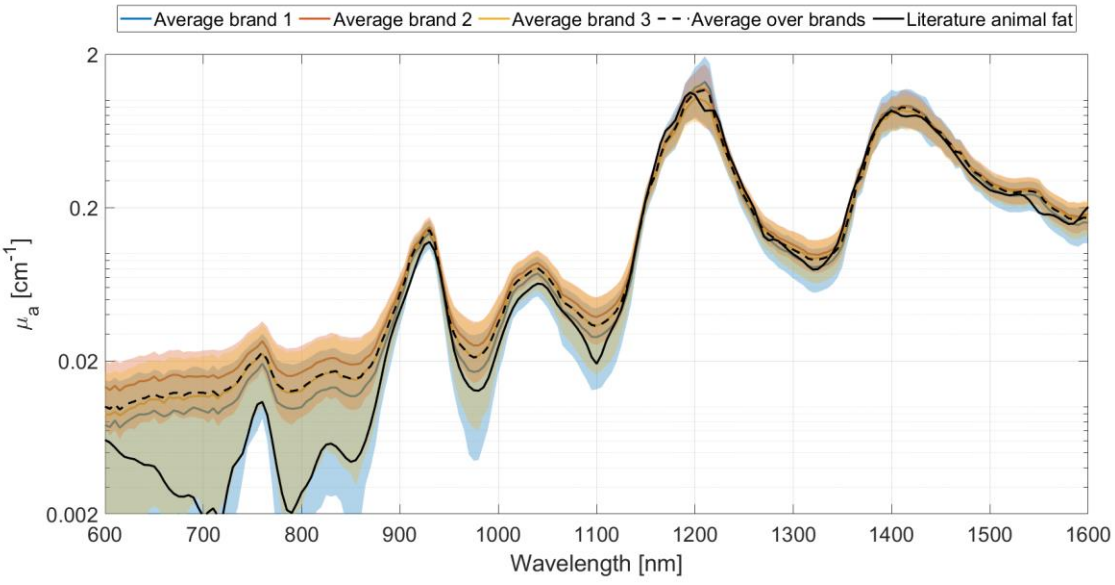

Figure 8: Comparison among fitted absorption spectra of different brands (blue, orange, yellow), average spectrum over brands (dotted black) and animal fat (solid black line) from 600 to 1600 nm.

Figure 8 also reports the absorption spectrum of animal fat, that is a reliable reference for lipids assessment.[49–52] Coconut oil has a consistent fatty acid profile and controlled antioxidant levels, despite some nutrient loss during mild processing.[53] It has the advantage to be cheap, easy to find at the supermarket, homogeneous and to enable the fabrication of complex structures in terms of shape and assembly (*e.g.*, inclusion in a homogeneous background, multilayer). Animal lard, instead, may vary due to biological and processing diversity. Differences might arise even within the same brand, depending on species, rendering method, and modifications such as hydrogenation or interesterification.[54,55] These factors could have an impact on the reproducibility in phantom preparation and measurements. In any case, our main goal is to propose a robust alternative, not a replacement, to animal fat, in order to offer more possibilities depending on material availability when it comes to tissue-mimicking phantom fabrication.

Comparing the average fitted absorption spectrum for coconut oil and the spectrum of animal fat, the ratio varies from 0.82 at 1360 nm (difference of -0.04 cm^{-1}) to 6.45 at 700 nm (difference of 0.01 cm^{-1}). Significant differences in absolute values occur in correspondence of the two highest absorption peaks. Animal fat attains a maximum at 1195 nm with μ_a=1.12 cm^{-1}, while method 2 identifies the corresponding maximum for coconut oil at 1210 with μ_a=1.17 cm^{-1}. Also, animal fat exhibits 2 maxima 1400 and 1425 nm, separated by a local minimum at 1415 nm, which does not take place for coconut oil. This could be not due only to chemical differences, but to technological limitations of the experimental setup, in particular the spectral resolution. It prevents to distinguish the narrow maximum-minimum-maximum sequence around 1400 nm, where spectral distances match the setup limit (in this range of about 10 nm).

After these considerations, the absorption spectrum averaged over brands obtained with method 2 has been selected as the reference for $\varepsilon_{coconut}$ in Eq. 2.

3.2 Validation of the optical properties of coconut oil

The coconut phantom was measured with the hyperspectral imaging setup described in Section 2.2.2. The resulting CW spectra were analysed via the approach illustrated in Section 2.2.3. For statistical relevance, the process was repeated for all spectra corresponding to a square area of 18 x 18 pixels in the centre of the image, in order to avoid boundary effects on the sample borders, minimize artefacts and enclose an area as homogeneous and uniform as possible.

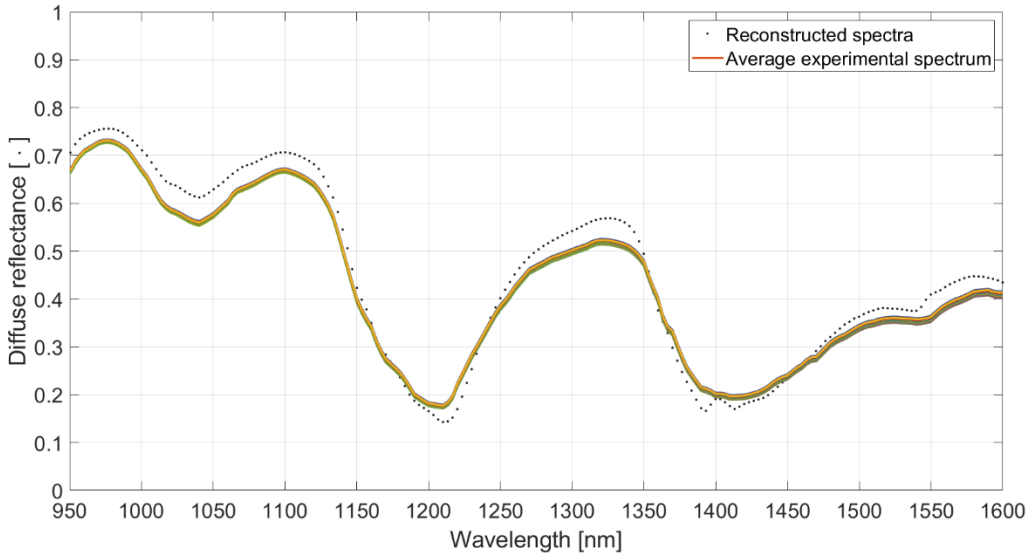

Figure 9: Example of comparison between the reconstructed (colourful solid lines) and the average experimental (black dotted line) coconut spectra. Each reconstructed spectrum corresponds to the application of the model to a pixel of the hyperspectral image.

Table 2: Average, standard deviation and 95% confidence intervals assuming normal or Beta distribution for the 4 fitting parameters, considering 324 pixels of a coconut phantom hyperspectral image. The phantom was measured on 3 different days.

	Day	Parameter	Average	Standard deviation	Confidence interval (Normal)	Confidence interval (Beta)
1	Day 1	**Coconut (%)**	99.0%	2.8%	[98.7%, 99.3%]	[91.3%, 100%]
		Water (%)	<0.001%	<0.001%	[<0.001%,<0.001%]	[<0.001%,<0.001%]
		a **(cm^{-1})**	8.55	0.31	[8.51, 8.58]	-
		b **(-)**	0.87	0.03	[0.869, 0.875]	-
2	Day 18	**Coconut (%)**	99.8%	0.5%	[99.7%, 99.8%]	[97.9%, 100%]

		Water (%)	<0.001%	<0.001%	[<0.001%,<0.001%]	[<0.001%,<0.001%]
		$\boldsymbol{a}$ **(cm^{-1})**	6.28	0.08	[6.28, 6.29]	-
		$\boldsymbol{b}$ **(-)**	0.59	0.02	[0.589, 0.594]	-
3	**Day 28**	**Coconut (%)**	99.0%	2.1%	[98.7%, 99.2%]	[90.4%, 100%]
		Water (%)	<0.001%	<0.001%	[<0.001%,<0.001%]	[<0.001%,<0.001%]
		$\boldsymbol{a}$ **(cm^{-1})**	6.92	0.15	[6.90, 6.93]	-
		$\boldsymbol{b}$ **(-)**	0.56	0.02	[0.559, 0.563]	-

Figure 9 depicts an exemplary comparison between the average experimental spectrum and the reconstructed spectra of 324 pixels derived with the model described above. Table 2 reports the average, standard deviation and the confidence intervals of the fitting parameters over the above-mentioned region of interest, for the 3 measuring days. To retrieve the confidence intervals, two different approaches were considered: a normal distribution (which does not take into account the physical bound of 100% as maximum concentration) and a Beta distribution (which is intrinsically bounded between 0 and 1 and may be skewed, especially near 0 or 1).[56]

Based on the product label, the phantom is made of pure coconut oil. Thus, we expect the fitting procedure to recognize it as 100% coconut oil. Indeed, averaging over pixels, data analysis recognizes a minimum average concentration of 99% of coconut. The deviation from 100% could be due to several reasons: (i) the previously mentioned broadband effect; (ii) the limited accuracy of the model of Flocke et al. for albedo values α close to 1 (errors lower than 10% for $\alpha > 0.95$,[47] when in our case this quantity ranges from 0.8978 to 0.9998, with the lowest values attained around 1200 nm and 1400 nm); (iii) the fact that we compared independent observations (coconut oils of different brands) obtained with 2 different techniques (time domain *vs* continuous wave). Also, the water content is always negligible, as expected, while the mean scattering amplitude and slope are respectively lower (6.28/8.55 cm^{-1} *vs* 16.67±3.58 cm^{-1}) and higher (0.56/0.87 vs 0.39±0.25) than the average values of Figure 4, most probably due to temperature mismatch caused by the heating from the illumination in the hyperspectral setup as compared to the fiber-based setup.

4 CONCLUSION

In conclusion, we presented the absorption and scattering spectra of coconut oil in the spectral range from 600 to 1600 nm. We used a time-resolved diffuse optical instrumentation, composed of a supercontinuum laser and a superconducting nanowire single photon detector. This work aims at emphasizing the use of coconut oil as fatty material for tissue-mimicking phantoms given its easy availability on the market and suitability to be moulded into various shapes, as a key part of the validation process of a diffuse optical system for biomedical applications.

We measured 15 coconut oil phantoms, combining 3 brands and 5 repetitions for robustness purposes.

While the scattering spectrum cannot be assumed as a fixed ground truth for future measurements given its significant dependence on temperature, the absorption spectrum could instead be considered as a reliable reference.

The experiments presented underlined the importance of the system spectral resolution for an accurate estimation of the optical properties.

Also, in correspondence of high absorption peaks, a coupling between absorption and scattering effects might arise. The results of a direct application of the diffuse model (method 1) could exhibit artefacts that affect the estimation of the coconut's optical properties. However, the absorption assessment benefits from the smoothing effect given by Mie's empirical law on the scattering spectrum, when a multi-stage analytical procedure is applied (method 2).

Even if improvable, the recovered absorption spectrum proved efficient to extrapolate the composition and microstructure of a homogeneous coconut oil phantom using a hyperspectral CW setup, recognizing on average a 99% coconut fraction over 324 pixels.

Therefore, future work could include new measurements with a setup with better spectral resolution. Also, a systematic study at different temperatures would be useful to complete a thorough optical assessment of coconut oil.

FUNDING

This work was partly supported by EU's HORIZON Europe Programme (fastMOT project) under Grant 101099291, by the European Union's NextGenerationEU Programme with the I-PHOQS Infrastructure [IR0000016, ID D2B8D520, CUP B53C22001750006] "Integrated infrastructure initiative in Photonic and Quantum Sciences" and by the National Plan for NRRP Complementary Investments (PNC, established with the decree-law 6 May 2021, n. 59, converted by law n. 101 of 2021) in the call for the funding of research initiatives for technologies and innovative trajectories in the health and care sectors (Directorial Decree n. 931 of 06-06-2022) - project n. PNC0000003 - CUP B53C22006720001 - AdvaNced Technologies for Human-centrEd Medicine (project acronym: ANTHEM).

DECLARATION OF CONFLICTING INTERESTS

The Authors declare that there is no conflict of interest.

RESEARCH DATA

The dataset gathered, analyzed, and discussed in this study is available in the Zenodo repository, 10.5281/zenodo.17610439. For any additional information please contact the corresponding author.

REFERENCES

1. Gibson A, Dehghani H. Diffuse optical imaging. *Philos Trans R Soc A Math Phys Eng Sci* 2009; 367: 3055–3072.
2. Hoshi Y, Yamada Y. Overview of diffuse optical tomography and its clinical applications. *J Biomed Opt* 2016; 21: 091312.
3. Durduran T, Choe R, Baker W, et al. Diffuse optics for tissue monitoring and tomography. *Reports Prog Phys* 2010; 73: 076701.
4. Mourant JR, Fuselier T, Boyer J, et al. Predictions and measurements of scattering and absorption over broad wavelength ranges in tissue phantoms. *Appl Opt* 1997; 36: 949.
5. Grosenick D, Rinneberg H, Cubeddu R, et al. Review of optical breast imaging and spectroscopy. *J Biomed Opt* 2016; 21: 091311.
6. Jakubowski DB, Cerussi AE, Bevilacqua F, et al. Monitoring neoadjuvant chemotherapy in breast cancer using quantitative diffuse optical spectroscopy: a case study. *J Biomed Opt* 2004; 9: 230.
7. Spliethoff JW, Prevoo W, Meier MAJ, et al. Real-time In Vivo Tissue Characterization with Diffuse Reflectance Spectroscopy during Transthoracic Lung Biopsy: A Clinical Feasibility Study. *Clin Cancer Res* 2016; 22: 357–365.
8. Zeng H, McWilliams A, Lam S. Optical spectroscopy and imaging for early lung cancer detection: a review. *Photodiagnosis Photodyn Ther* 2004; 1: 111–122.
9. Baltussen EJM, Brouwer de Koning SG, Sanders J, et al. Tissue diagnosis during colorectal cancer surgery using optical sensing: an in vivo study. *J Transl Med* 2019; 17: 333.
10. Brouwer de Koning SG, Baltussen EJM, Karakullukcu MB, et al. Toward complete oral cavity cancer resection using a handheld diffuse reflectance spectroscopy probe. *J Biomed Opt* 2018; 23: 1.

11. Fei B, Lu G, Wang X, et al. Label-free reflectance hyperspectral imaging for tumor margin assessment: a pilot study on surgical specimens of cancer patients. *J Biomed Opt* 2017; 22: 1.
12. Torricelli A, Contini D, Pifferi A, et al. Time domain functional NIRS imaging for human brain mapping. *Neuroimage* 2014; 85: 28–50.
13. Vandebriel R, Luthman S, Vunckx K, et al. Integrating hyperspectral imaging in an existing intra-operative environment for detection of intrinsic brain tumors. In: Boudoux C, Tunnell JW (eds) *Advanced Biomedical and Clinical Diagnostic and Surgical Guidance Systems XXI*. SPIE, p. 33.
14. Eggebrecht AT, Ferradal SL, Robichaux-Viehoever A, et al. Mapping distributed brain function and networks with diffuse optical tomography. *Nat Photonics* 2014; 8: 448–454.
15. Yu G, Durduran T, Lech G, et al. Time-dependent blood flow and oxygenation in human skeletal muscles measured with noninvasive near-infrared diffuse optical spectroscopies. *J Biomed Opt* 2005; 10: 024027.
16. Hu G, Zhang Q, Ivkovic V, et al. Ambulatory diffuse optical tomography and multimodality physiological monitoring system for muscle and exercise applications. *J Biomed Opt* 2016; 21: 1.
17. Zhao F, Levoni P, Frabasile L, et al. Reproducibility of identical solid phantoms. *J Biomed Opt* 2022; 27: 1–13.
18. Pifferi A, Torricelli A, Bassi A, et al. Performance assessment of photon migration instruments: the MEDPHOT protocol. *Appl Opt* 2005; 44: 2104.
19. Ferocino E, Di Sciacca G, Di Sieno L, et al. Multi-wavelength time domain diffuse optical tomography for breast cancer: initial results on silicone phantoms. 2019; 59.
20. Waks Serra MV, Noseda Grau V, Vera DA, et al. Anthropomorphic Polydimethylsiloxane silicone-based phantom for Diffuse Optical Imaging. *Heliyon* 2022; 8: e10308.
21. Martelli F, Ninni P Di, Zaccanti G, et al. Phantoms for diffuse optical imaging based on totally absorbing objects, part 2: experimental implementation. *J Biomed Opt* 2014; 19: 076011.
22. Spinelli L, Botwicz M, Zolek N, et al. Determination of reference values for optical properties of liquid phantoms based on Intralipid and India ink. *Biomed Opt Express* 2014; 5: 2037.
23. Lepore M, Delfino I. Intralipid-Based Phantoms for the Development of New Optical Diagnostic Techniques. *Open Biotechnol J* 2019; 13: 163–172.
24. Flock ST, Jacques SL, Wilson BC, et al. Optical properties of intralipid: A phantom medium for light propagation studies. *Lasers Surg Med* 1992; 12: 510–519.
25. Dempsey LA, Persad M, Powell S, et al. Geometrically complex 3D-printed phantoms for diffuse optical imaging. *Biomed Opt Express* 2017; 8: 1754.
26. Diep P, Pannem S, Sweer J, et al. Three-dimensional printed optical phantoms with customized absorption and scattering properties. *Biomed Opt Express* 2015; 6: 4212.
27. Amendola C, Lacerenza M, Pirovano I, et al. Optical characterization of 3D printed PLA and ABS filaments for diffuse optics applications. *PLoS One* 2021; 16: e0253181.
28. Ferocino E, Di Sciacca G, Di Sieno L, et al. Spectral approach to time domain diffuse optical tomography for breast cancer: validation on meat phantoms. In: Dehghani H, Wabnitz H (eds) *Diffuse Optical Spectroscopy and Imaging VII*. SPIE, p. 7.
29. Jacques SL. Corrigendum: Optical properties of biological tissues: a review. *Phys Med Biol* 2013; 58: 5007–5008.
30. Pogue BW, Patterson MS. Review of tissue simulating phantoms for optical spectroscopy, imaging and dosimetry. *J Biomed Opt* 2006; 11: 041102.
31. Hacker L, Wabnitz H, Pifferi A, et al. Criteria for the design of tissue-mimicking phantoms for the standardization of biophotonic instrumentation. *Nat Biomed Eng* 2022; 6: 541–558.
32. Rajaa Nader K. Spectral and Nonlinear Properties of Coconut Oil. *J Phys Conf Ser* 2021; 2114: 012035.
33. Rohman A. Infrared spectroscopy for quantitative analysis and oil parameters of olive oil and virgin coconut oil: A review. *Int J Food Prop* 2017; 20: 1447–1456.
34. Rajamani AS, Shamlee JK, Rammohan A, et al. Diffuse Reflectance Spectroscopy for The

Assessment of Steatosis in Liver Phantom and Liver Donors - A Pilot Study. *2022 44th Annu Int Conf IEEE Eng Med Biol Soc* 2022; 3003–3006.
35. Cannatà A, Meo S Di, Matrone G, et al. Multimodal tissue-mimicking breast phantoms for mm-wave and ultrasound imaging. DOI: 10.23919/EuCAP57121.2023.10133246.
36. Losch MS, Kardux F, Dankelman J, et al. Diffuse reflectance spectroscopy of the spine: improved breach detection with angulated fibers. *Biomed Opt Express* 2023; 14: 739.
37. Yang D, Lee YY, Lu Y, et al. Internal Factors Affecting the Crystallization of the Lipid System: Triacylglycerol Structure, Composition, and Minor Components. *Molecules*; 29. Epub ahead of print 2024. DOI: 10.3390/molecules29081847.
38. Michel N, Fabiano AS, Polidori A, et al. Determination of phase transition temperatures of lipids by light scattering. *Chem Phys Lipids* 2006; 139: 11–19.
39. Pifferi A, Contini D, Dalla Mora A, et al. New frontiers in time-domain diffuse optics, a review. *J Biomed Opt* 2016; 21: 091310.
40. Hisham A. Maddah. Polypropylene as a Promising Plastic: A Review. *Am J Polym Sci* 2016; 6: 1–11.
41. Martelli F, Del Bianco S, Ismaelli A, et al. *Light Propagation through Biological Tissue and Other Diffusive Media: Theory, Solutions, and Software*. 1000 20th Street, Bellingham, WA 98227-0010 USA: SPIE. Epub ahead of print 23 December 2009. DOI: 10.1117/3.824746.
42. Mat Yunus WM, Fen YW, Yee LM. Refractive Index and Fourier Transform Infrared Spectra of Virgin Coconut Oil and Virgin Olive Oil. *Am J Appl Sci* 2009; 6: 328–331.
43. Kho E, de Boer LL, Post AL, et al. Imaging depth variations in hyperspectral imaging: Development of a method to detect tumor up to the required tumor-free margin width. *J Biophotonics* 2019; 12: 1–12.
44. Kho E, Dashtbozorg B, Sanders J, et al. Feasibility of Ex Vivo Margin Assessment with Hyperspectral Imaging during Breast-Conserving Surgery: From Imaging Tissue Slices to Imaging Lumpectomy Specimen. *Appl Sci* 2021; 11: 8881.
45. Jong L-JS, de Kruif N, Geldof F, et al. Discriminating healthy from tumor tissue in breast lumpectomy specimens using deep learning-based hyperspectral imaging. *Biomed Opt Express* 2022; 13: 2581.
46. Kho E, Dashtbozorg B, de Boer LL, et al. Broadband hyperspectral imaging for breast tumor detection using spectral and spatial information. *Biomed Opt Express* 2019; 10: 4496.
47. Flock ST, Patterson MS, Wilson BC, et al. Monte Carlo Modeling of Light Propagation in Highly Scattering Tissues—I: Model Predictions and Comparison with Diffusion Theory. *IEEE Trans Biomed Eng* 1989; 36: 1162–1168.
48. Faber DJ, Aalders MCG, Mik EG, et al. Oxygen Saturation-Dependent Absorption and Scattering of Blood. *Phys Rev Lett* 2004; 93: 028102.
49. Nachabé R, Hendriks BHW, Desjardins AE, et al. Estimation of lipid and water concentrations in scattering media with diffuse optical spectroscopy from 900 to 1600 nm. *J Biomed Opt* 2010; 15: 037015.
50. van Veen RLP, Sterenborg HJCM, Pifferi A, et al. Determination of visible near-IR absorption coefficients of mammalian fat using time- and spatially resolved diffuse reflectance and transmission spectroscopy. *J Biomed Opt* 2005; 10: 054004.
51. van Veen RLP, Sterenborg HJCM, Pifferi A, et al. Optical Absorption of Fat, https://omlc.org/spectra/fat/ (accessed 22 June 2023).
52. Damagatla V, Boetti NG, Di Sieno L, et al. Bioresorbable fibers for interstitial null-separation diffuse optical spectroscopy using fast temporal gating. *JPhys Photonics*; 7. Epub ahead of print 2025. DOI: 10.1088/2515-7647/ada656.
53. Liu R, Guo X, Cheng M, et al. Effects of chemical refinement on the quality of coconut oil. *J Food Sci Technol* 2019; 56: 3109–3116.
54. Marikkar JMN, Yanty NAM. Effect of Chemical and Enzymatic Modifications on the Identity Characteristics of Lard: A Review. *Int J Food Prop* 2014; 17: 321–330.

55. Segura J, Rey AI, Olivares Á, et al. Free-Range Feeding Alters Fatty Acid Composition at the sn-2 Position of Triglycerides and Subcutaneous Fat Physicochemical Properties in Heavy Pigs. *Animals* 2021; 11: 2802.
56. Hammouri HM, Sabo RT, Alsaadawi R, et al. Handling skewed data: A comparison of two popular methods. *Appl Sci*; 10. Epub ahead of print 2020. DOI: 10.3390/APP10186247.